Magnetic Oleosome as a Functional Lipophilic Drug Carrier for Cancer Therapy

Hyeon-Yeol Cho,[†,‡,#] Taek Lee,[†,§,#] Jinho Yoon,[†] Zhenlin Han,[∥] Hudifah Rabie,[‡] Ki-Bum Lee,[‡,⊥] Wei Wen Su,*[,∥] and Jeong-Woo Choi*[,†]

[†]Department of Chemical & Biomolecular Engineering, Sogang University, Seoul 04107, Korea

[‡]Department of Chemistry and Chemical Biology, Rutgers, The State University of New Jersey, Piscataway, New Jersey 08854, United States

[§]Department of Chemical Engineering, Kwangwoon University, Seoul 01897, Korea

[∥]Department of Molecular Biosciences and Bioengineering, University of Hawaii at Manoa, Honolulu, Hawaii 96822, United States

[⊥]College of Pharmacy, Kyung Hee University, Seoul 02447, Korea

S Supporting Information

ABSTRACT: In the present study, we fabricated magnetic oleosomes functionalized with recombinant proteins as a new carrier for oil-based lipophilic drugs for cancer treatment. The bioengineered oleosome is composed of neutral lipids surrounded by a phospholipid monolayer with embedded oleosin fusion proteins. The oleosin was genetically fused to a nanobody of a green fluorescent protein (GFP). A recombinant protein consisting of immunoglobulin-binding protein LG fused to GFP was used to couple the oleosome to an antibody for targeted delivery to breast cancer cells. The lipid core of the oleosome was loaded with magnetic nanoparticles and carmustine as the lipophilic drug. The magnetic oleosome was characterized using transmission electron microscopy and dynamic light scattering. Moreover, the specific delivery of oleosome into the target cancer cell was investigated via confocal microscopy. To examine the cell viability of the delivered oleosome, a conventional 3-(4,5-dimethylthiazol-2-yl)-2,5-diphenyltetrazolium bromide assay was carried out. Furthermore, an animal study was conducted to confirm the effect resulting from the delivery of the anticancer drug-loaded oleosomes. Taken together, the fabricated lipophilic drug-loaded magnetic oleosome can be a powerful tool for oil-based drug delivery agent for cancer therapy.

KEYWORDS: oleosome, lipophilic drug delivery, magnetic hyperthermia, cancer therapy, carmustine
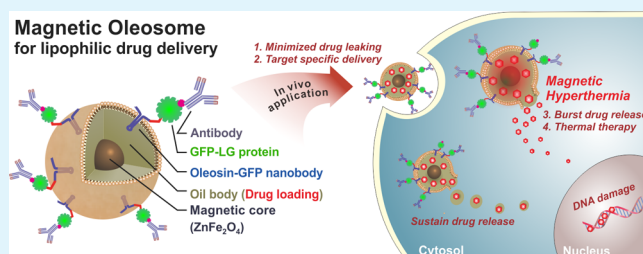
■ INTRODUCTION

Numerous potent lipophilic drugs exhibit low bioavailability and cannot be delivered by oral or intravenous injection routes of administration in their original form due to instability, low membrane permeability, poor solubility, efflux transport mechanisms, etc.[1,2] In recent years, lipid-based formulations have been used to improve the bioavailability of lipophilic drug compounds, which include micro- or nanoemulsions,[3−5] self-emulsifying formulations,[6] surfactant dispersions,[7] liposomes,[8,9] and solid lipid nanoparticles.[10,11] Nanoemulsions offer several advantages including enhanced solubility, rapid onset of action (no extra time for dispersion), reduced intersubject variability, toxicological safety, and a high content of the lipid phase.[12,13] The decrease in the rate of dissolution of self-emulsifying drug delivery systems may lower the potential of the lipophilic drug delivery system compared to a liquid micro/nanoemulsion. Additionally, administration of a lipophilic compound in a dissolved state and in a liquid formulation can reduce the energy associated with the solid−liquid transition.[14] For example, to improve the stability of the lipophilic drug in the water phase, liposomes are popularly utilized by incorporating active lipophilic components into inert lipid bilayers.[15] However, this technique has a limitation in its limited drug-loading capacity considering that lipophilic drugs can exist in stable conditions only inside the lipid bilayer.[16] To overcome this limitation, amphiphilic polymer-based micro/nanoemulsion systems were recently proposed; however, although holding great potential, their biodegradability remains a lasting concern.

The oleosomes, oil body encapsulating vesicles, are another example of naturally occurring structures that are engineered by natural self-assembly.[17,18] The structure of an oleosome is that of oil droplets surrounded by a monolayer of phospholipids embedded with some unique proteins such as oleosin. These naturally occurring oil droplet structures are quite unique because they do not aggregate or coalesce, even when subjected
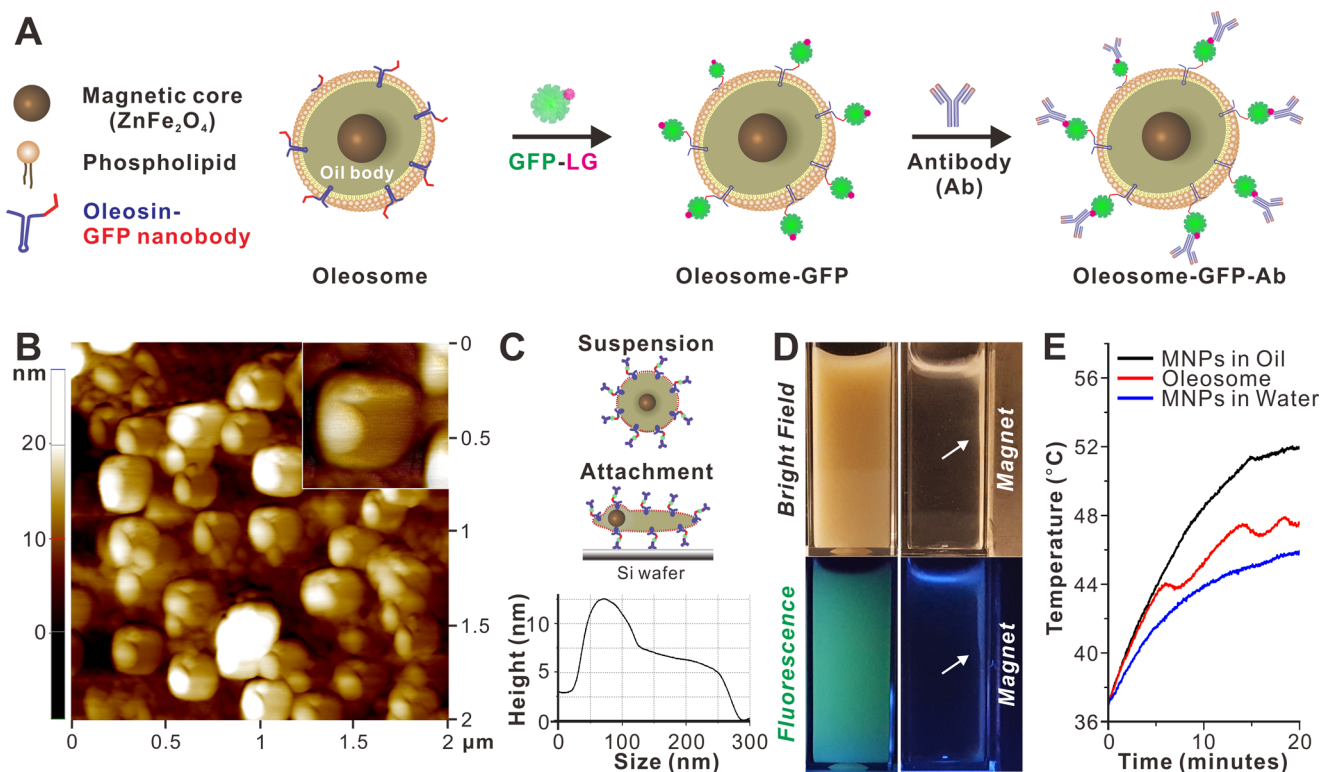
Figure 1. Synthesis and characterization of functional oleosome. (A) The functional oleosome are synthesized by four steps. Step 1: synthesis of zinc-doped magnetic nanoparticles ($ZnFe_2O_4$, MNPs, 8 nm) and dispersion in olive oil. Step 2: adding phosphate-buffered saline (PBS) solution containing the phospholipid and oleosin-green fluorescent protein (GFP) nanobody into olive oil containing MNP and forming the oleosome with ultrasonication. Step 3: GFP labeling of oleosome by conjugation of GFP-LG protein with oleosin-GFP nanobody. Step 4: providing target-specific moiety to oleosome by antibody conjugation with GFP-LG protein. (B) Atomic force microscopy (AFM) image of oleosomes (inset: size of x-, y-axis = 400 nm) and (C) cross-sectional measurement along the line shown in inset in (B). (D) Representative picture showing that the oleosomes dispersed in water are attracted to a magnet. (E) The MNPs-containing solutions (oil and water) and magnetic oleosome in water (100 μg/mL) exhibited an elevated temperature when exposed to an alternating magnetic field (AMF), exhibiting the localized heating effect. The temperature was monitored using a fiber-optic probe.

to extreme environmental stresses, such as moisture or temperature fluctuations.[19] Moreover, they retain their structural integrity and stability even after they have been extracted from the seed. However, the sizes exhibited by natural oleosomes are relatively big, i.e., 0.5−2.0 μm, and therefore are limited in their application as intracellular drug delivery vehicles. Furthermore, an additional modification is often needed to give target specificity as well as additional functionality.[19,20]

To address the aforementioned lipophilic drug delivery challenges, here, we first demonstrate a nanosized functional oleosome capable of specifically targeting lipophilic drug delivery and inducing magnetic hyperthermia. The functional oleosome is composed of a highly magnetic zinc-doped iron oxide ($ZnFe_2O_4$) nanoparticle core in the oleosome inner space, an amphiphilic recombinant peptide (oleosin fusion protein), an oil body (olive oil), and an antibody surface functionalization. Our unique oleosin fusion protein design enables easy and efficient coupling of the targeting antibodies with oleosome via self-assembly. Moreover, the multifunctionality of our oleosome allows for the induction of magnetic hyperthermia via exposure to an alternating magnetic field (AMF) to further sensitize cancer cells to subsequent chemotherapy. Figure 1A shows the oleosome fabrication steps.

EXPERIMENTAL SECTION

Materials. 3-(4,5-Dimethylthiazol-2-yl)-2,5-diphenyltetrazolium bromide (MTT) and olive oil were purchased from Sigma-Aldrich. Purchased from Sigma-Aldrich, phosphate-buffered saline (PBS) was prepared in deionized (DI) water. The washing buffer was prepared by 50 mM Tris, 150 mM sodium chloride, 0.02% dodecyl maltoside, and 20 mM imidazole. The elution buffer was composed of 50 mM Tris, 150 mM sodium chloride, 0.02% dodecyl maltoside, and 250 mM imidazole. Sodium chloride, Tris and dodecyl maltoside, and dimethyl sulfoxide (DMSO) was purchased from Daejung Chemical (Korea). Nitrosonium tetrafluoroborate ($NOBF_4$) and imidazole were obtained from Sigma-Aldrich. The 1,2-dioleoyl-*sn*-glycero-3-phosphocholine used as phospholipid was purchased from Sigma-Aldrich. Ni-nitrilotriacetic acid (NTA) resin for affinity chromatography was purchased from Qiagen (Germany). To pull the MNP, MagCellect magnet was obtained from R&D systems.

Construction of Plasmids for Expressing OHNG and GFP-LG Fusion Proteins. Two recombinant fusion proteins, oleosin fused with anti-GFP nanobody via a cellulosomal hydrophilic domain (HD) linker (Oleosin-HD linker-Nanobody of GFP, OHNG) and protein LG fused with GFP (GFP-LG), were produced using *Escherichia coli*. To construct the plasmid pET-OHNG encoding oleosin-HD-nanobody with a C-terminal His-tag, a GFP-nanobody fragment was amplified with forward primer NGB (5′-cgcggatcccaggttcaactggtggaaag-3′; *Bam*HI site underlined) and a reverse primer XGR (5′-cgcctcgagttagtgatggtgatg-3′; *Xho*I site underlined) using the plasmid pCTNG[21] as the template. The resulting polymerase chain reaction (PCR) product was digested with *Bam*HI and *Xho*I and ligated into *Bam*HI-*Xho*I linearized pET21a(+) to form pETNG. Subsequently,

the olesin−HD fusion fragment was PCR amplified with forward primer OXF (5′-aatgtctagagctgagcattatggtcaaca-3′; *Xba*I site underlined) and reverse primer HDRB (5′-cgcagatctgccagggatatcttttggtaa-3′; *Bgl*II site underlined) using pOHC[22] as the template, digested with *Xba*I and *Bgl*II, and subcloned into *Nhe*I-*Bam*HI linearized pETNG to create pET-OHNG. Plasmid pET-GFP-LG encodes immunoglobulin-binding protein LG from Peptostreptococcus magnus fused with a His$_6$-tagged GFP. It was assembled via two-step cloning. First, LG coding sequence was amplified from pHD389-LG[23] using forward primer LGF (5′-catatggctagcaaaaaaactgctatcgctatc-3′; *Nhe*I site underlined) and reverse primer LGR (5′-atcgagctcatttcagttaccgtaaagg-3′; *Sac*I site underlined). The obtained LG fragment was integrated into *Nhe*I-*Sac*I linearized pET21a(+) to form pETLG. Then the DDDDKGGR-GFP-His$_6$ coding sequence was obtained by PCR from pH469 (provided by H. Edske) with forward primer GFS (5′-cgcgagctcgatgacgacgacaagggcg-3′; *Sac*I site underlined) and reverse primer XGR; it was digested with *Sac*I and *Xho*I and ligated into pETLG to form pET-GFP-LG.

Magnetic Nanoparticle Synthesis. The synthesis of ZnFe$_2$O$_4$ magnetic nanoparticles (MNPs) has previously been reported and modified by our group.[24−28] Briefly, 1.35, 0.3, and 0.7 mM of Fe(acac)$_3$, ZnCl$_2$, and FeCl$_2$, respectively, were mixed into a round-bottom flask with 20 mL of tri-*n*-octylamine, 6 mM of both oleic acid and oleylamine, and 10 mM of 1,2-hexadecanediol. The reaction mixture was then heated, at a rate of 4 °C/min, up to 200 °C for 2 h. From here, the mixture was heated to 305 °C, using a similar heating rate, for another 2 h and the nanoparticles were purified by repeatedly washing with ethanol. Finally, the MNPs were characterized via transmission electron microscopy (TEM) using a JEOL 1200EX electron microscope model at 80.0 kV.

To characterize the magnetic properties of the nanoparticles, the resulting MNPs (25 μg/mL in olive oil) were exposed to an AMF (5 kA/m, 225 kHz) using a solid-state induction heating system (Superior Induction Company) for 1 h. The temperature of the solution was monitored using a fiber-optic temperature probe (LumaSense Technologies). The scanning transmission electron microscopy (STEM) image was obtained using a Nion UltraSTEM microscope (Nion) using an electron probe with a convergence semiangle of 35 mrad. Powder crystal diffraction data was recorded using an Ultima IV X-ray diffractometer (Rigaku) a with Cu Kα radiation (λ = 1.5406 Å). Data were collected between 18 and 70° 2θ with a step size of 0.02° and a scan speed of 2°/min.

For the specific heat capacity experiment, hydrophilic ZnFe$_2$O$_4$ MNPs also were prepared via ligand exchange using NOBF$_4$.[29] Briefly, 1 mL of a hydrophobic MNP dispersion in hexane (5 mg/mL) was mixed with 1 mL of a dichloromethane solution of NOBF$_4$ (0.01 M) at room temperature. After 5 min, precipitated MNPs were obtained by centrifugation and redispersed in the dimethylformamide (DMF). To purify the hydrophilic MNPs, the same volume of the hexane was added to the MNP solution in DMF and mixed. The MNPs were then precipitated with centrifugation, followed by the addition of a small volume of DMF (100 μL) to redisperse the hydrophilic MNPs, which were then diluted in DI water (5 mg/mL as the final concentration in DI water).

Purification of Recombinant Proteins. Recombinant His-tagged GFP-LG fusion protein was expressed in *E. coli* and purified using immobilized metal affinity chromatography with Ni-NTA in the batch mode. Eluted GFP-LG protein solution was further processed using centrifugal ultrafiltration membrane tubes to remove imidazole. Finally, the recombinant GFP-LG was obtained. To purify the recombinant OHNG protein, a frozen pellet of the cell for oleosin was diluted in PBS, and then, following the same process of the recombinant GFP-LG purification. The purified GFP-LG and OHNG proteins were checked using 12% sodium dodecyl sulfate polyacrylamide gel electrophoresis.

Synthesis and Characterization of Functional Oleosome. To synthesize the oleosome, MNPs were dried and dispersed in the olive oil (1 mg/mL). For cancer treatment, carmustine was dispersed (solubility in olive oil: 300 mg/mL) along with the MNP in the olive oil, inside the oleosome with different concentrations (0, 2.5, 5, 10,

and 20 μM). The recombinant OHNG was prepared in a PBS (10 mM, pH 7.2). The OHNG solution was mixed with the MNP and carmustine olive oil solution for 5 min on ice, followed by sonication via an ultrasonicator three times, using 20 kHz, 5 Watts for 30 s. After sonication, an emulsion-like structure (oleosome) was synthesized, which composed of an inner olive oil component possessing the MNP and a water-soluble outer component. To wash and purify the oleosomes in the mixed solution, the oleosomes were pulled by a magnet utilizing the encapsulated MNP inside the oleosome, after which, the fresh buffer solution was used to wash the oleosomes several times. After the washing, 100 μg of phospholipid was dispersed in PBS (100 μg/mL as a final concentration in the oleosome solution), which was then added to the oleosome solution, followed by sonication. The solution was sonicated with an ultrasonicator using 20 kHz, 5 Watts for 30 s, followed by washing with fresh buffer using an external magnet as described previously, resulting in our MNP and carmustine-loaded oleosome. Hundred microlitres of recombinant GFP-LG (1 mg/mL) was then immobilized on the fabricated oleosome. Finally, the MNP and carmustine-loaded oleosome with GFP-LG functionalization for cancer treatment were fabricated. The constructed oleosome was investigated by TEM, and the fully functionalized oleosomes were characterized by atomic force microscopy (AFM), TEM, dynamic light scattering (DLS), and ζ-potential analysis. The AFM images were obtained by using NX-10 (Park systems) with a tapping mode using 0.3 Hz scan rate for selected area. The TEM images were acquired by using a JEOL transmission electron microscope (JEM1010) with an accelerating voltage of 80 kV. The DLS and ζ-potential analysis were performed using a Malvern Instruments Zetasizer Nano ZS-90 instrument (Southboro, MA) with reproducibility being verified by the collection and comparison of sequentially obtained measurements. Oleosomes were prepared using purified water (resistivity = 18.5 MΩ cm). The DLS measurements were performed at a 90° scattering angle at 25 °C. The Z-average sizes of three sequential measurements were collected and analyzed. The ζ-potential measurements were collected at 25 °C, and the Z-average potentials following three sequential measurements were collected and analyzed.

Specific Cell Targeting with Functional Oleosome. Twenty-four hours before the functional oleosome treatment, breast cancer cells (MDA-MB-231 and SK-BR-3 from the Korean cell line bank) and human mammary epithelial cells (HMECs, from Lonza) were seeded into each well of a 6 well plate, so as to attain 70% confluency at the time of transfection. The functional oleosomes were formed as described above. Thereafter, various concentrations of oleosomes solutions were prepared in PBS and added to each well to measure dose efficiency. Subsequently, the cell culture plates were placed on a static magnetic plate (R&D systems) for 2 h and afterward the cells were washed with PBS and the transfection medium was replaced with fresh growth medium. The growth mediums for the cell lines (obtained from Gibco) used in the study are as follows: Roswell Park Memorial Institute 1640 supplemented with 10% FBS and 1% Penicillin−Streptomycin.

In Vitro Cell Viability Assay. To test the anticancer drug-containing oleosome, an MTT assay was conducted. 2×10^4 cells were seeded with 100 μL growth media and incubated in a 96 well plate to validate the results of the oleosome drug delivery. After 24 h, the media in the plates were changed to fresh media and 10 μL of carmustine-loaded oleosome solution was added. The oleosome-treated cells were incubated for an additional 24 h while being mounted onto a magnetic plate as described before to assist in MNP-mediated oleosome transfection. MTT solution (20 μL) was added to each well and incubated for 2 h in 37 °C. The solutions in the wells were replaced with 100 μL of DMSO and incubated for 20 min. As the final step, the cell viability was monitored by taking 540 nm absorbance measurements using a Benchmark microplate reader (Bio-Rad, Canada). The percentage of viable cells was normalized by a control (10 μL PBS treated) condition as 100% viable. All measurements were made 48 h after initial transfection. All experiments were conducted five times (n = 5) and averaged.
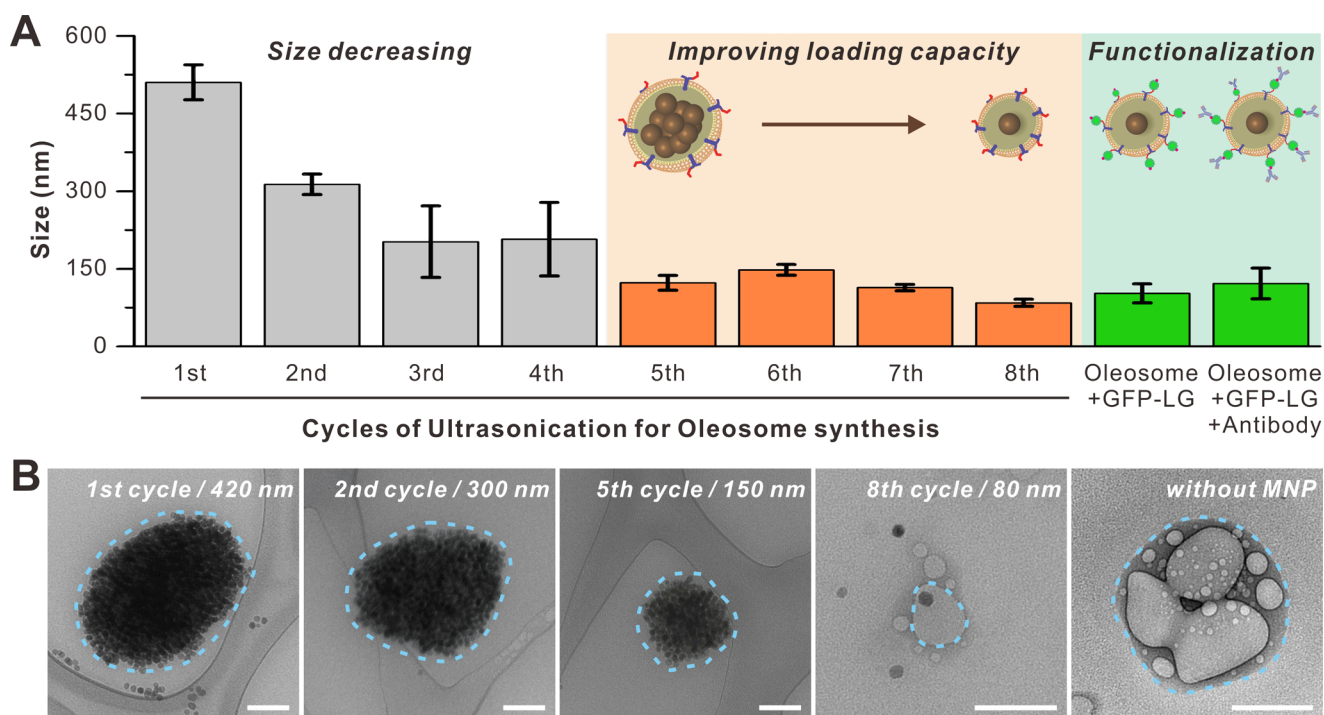
Figure 2. Optimization of oleosome synthesis. (A) Size distribution of functional oleosomes in the synthesis process. The size of oleosome was decreased with two different phases by repentance of ultrasonication. In the first phase of ultrasonication (1st to 5th repentance), the size of oleosomes was decreased, but the inside of oleosome was filled up with MNPs. Afterward, in the second phase, the size of oleosomes was saturated and the number of inner MNPs was decreased. After eighth cycle of ultrasonication, oleosome was functionalized with GFP-LG protein and antibody. Values are given as mean ± scanning electron microscopy (SEM). (B) Transmission electron microscopy images of oleosomes in each step. Dash line is the border of oleosome. Scale bar is 100 nm.

Magnetic Hyperthermia. Twenty-four hours after transfection, cells were washed with Dulbecco's phosphate-buffered saline, trypsinized, and exposed to an AMF (5 kA/m, 225 kHz) for the desired amount of time. In particular, to achieve a constant temperature of 45 °C, the cells were initially exposed to an AMF for 15 min to achieve a temperature of 45 °C. Afterward, the cells were periodically exposed to AMF (5 min on, 2 min off, three cycles) to maintain the temperature at 45 °C. Thereafter, fresh media was added to the treated cells and the cells were plated back into 24 well plates. Every procedure was conducted for the control group with the same time conditions.

Fluorescence-Based Monitoring of Lipophilic Drug Release. The green fluorescent, lipophilic carbocyanine SP-DiOC$_{18}$(3) was selected as a model to monitor the release of the lipophilic drugs from oil to the water phase. SP-DiOC$_{18}$(3) is a DiO analogue that contains sulfonate groups that improve the water solubility while maintaining the similar water solubility to carmustine (4 mg/mL).[30] Before testing with the oleosome, SP-DiOC$_{18}$(3) was dissolved in water with different concentrations (0−40 μM) and its fluorescent intensities were measured with a fluorescence spectrophotometer (Cary Eclipse Fluorescence Spectrophotometer, Agilent) with fixed excitation (497 nm) and emission (513 nm) wavelengths to generate a standard curve. After the standard curve plotting, an oleosome containing 20 μM SP-DiOC$_{18}$(3) in olive oil was synthesized. The oleosome solution was mixed with PBS and the fluorescent signal of this solution was measured at different time points (0, 0.5, 1, 2, 4, 6, 12, 24, and 36 h). To measure the fluorescent signal of PBS, oleosome-mixed PBS was separated by centrifugation (6000 rpm, 5 min).

Animal Studies. The xenograft mouse model was generated by transplanting malignant breast cancer cells (MDA-MB-231) into 5-week-old female BALB/c nude mice (SLC, Japan). All animals were acclimated to the animal facility for 7 days before experimentation and maintained according to the Guide for the Care and Use of Laboratory Animals published by the National Institute of Health. They were housed in a barrier under high-efficiency particulate air filtration and provided with sterilized food and water ad libitum. The animal facility was kept under 12 h light/dark cycles at room temperature 21 ± 2 °C with 30−40% humidity. Approximately 2.0 × 10^6 MDA-MB-231 cells were mixed with 354234-matrigel (BD) and subcutaneously injected into the dorsal area of mice. Cancer cell-transplanted mice (n = 15) were monitored daily and separated into three groups based on the size of the tumor when more than 60% of mice had around 100 mm^3 tumor volume. Three different treatment conditions were designed to evaluate the anticancer effect of the functional oleosomes: group 1 (G1): negative control (PBS); group 2 (G2): positive control (carmustine with PBS); and group 3 (G3): functional oleosome groups. The treatments were performed once every 3 days (two times a week) via intravenous injection and the injection volume was 50 mL/kg. The treated concentration of carmustine was 0.428 mg/kg for G2 and G3. The animals were also weighed two times a week. After 4 weeks, the tumors were extracted after euthanasia.

RESULTS AND DISCUSSION

Formation of Functional Oleosome. To fabricate functional oleosomes, several steps were required. Figure 1A illustrates a schematic representation of the fabrication process. First, we have synthesized magnetic nanoparticles with a composition of ZnFe$_2$O$_4$, which has a higher magnetic susceptibility compared to the Fe$_2$O$_3$ or Fe$_3$O$_4$ nanoparticles, characterizing their size and morphology using TEM.[28,31,32] To further characterize the nanoparticles, we measured a d-spacing of approximately 0.16 Å, corresponding to the (511) lattice place, which is a representative structural information for zinc-doped magnetic nanoparticles obtained using STEM (Figure S1). The elemental composition of ZnFe$_2$O$_4$ nanoparticles is obtained from energy-dispersive X-ray spectroscopy. The peaks corresponding to Fe (6.405 keV) and Zn (8.637 keV) are observed in the ZnFe$_2$O$_4$ nanoparticle sample, whereas Fe$_3$O$_4$
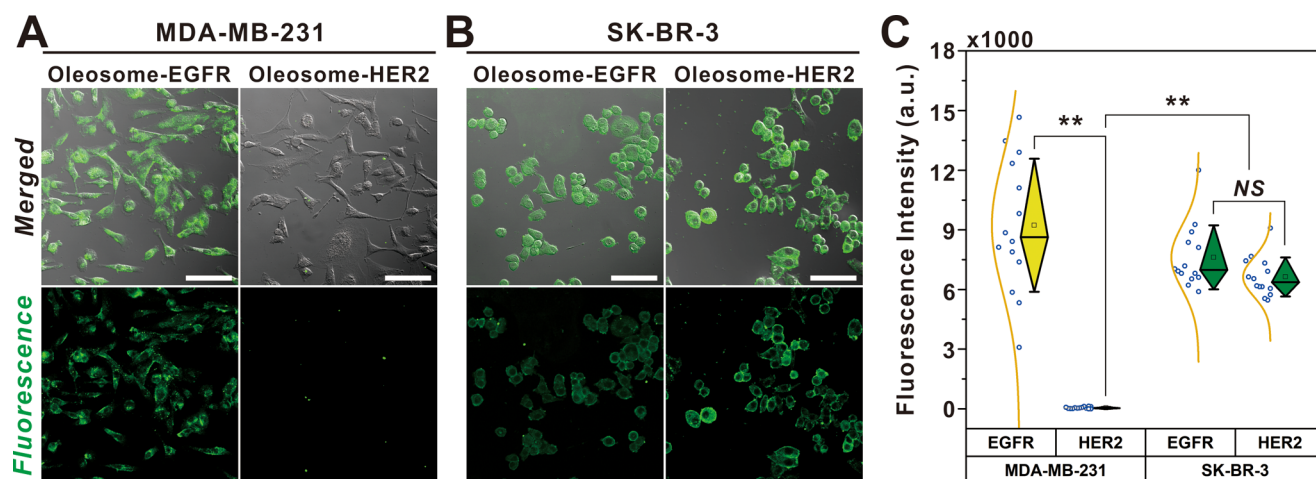
Figure 3. Specific targeting property of functional oleosome. Two different oleosomes were functionalized with two antibodies (EGFR and HER2) and tested with cancer cells. The green fluorescence signal of GFP-LG protein on oleosome was utilized as an indicator of oleosome labeled cells. (A) MDA-MB-231 cells were labeled with oleosome-EGFR but not with oleosome-HER2. (B) SK-BR-3 cells were labeled with both oleosome-EGFR and oleosome-HER2. Images in the upper row are merged images of phase and fluorescence images and those in the bottom row are fluorescence images. Fluorescence images were obtained with fluorescein isothiocyanate filter (495 nm excitation, 520 nm emission). Scale bar is 100 μm. (C) Normalized fluorescence intensity of functional oleosome treated cancer cells. **$p < 0.0001$.

sample showed only Fe (Figure S2). The magnetic nanoparticles, phospholipid, and purified oleosin fusion protein were mixed and ultrasonicated several times. The LG-GFP fusion protein was then introduced to self-assemble with the nanobody on the oleosome surface. In the final step, the epidermal growth factor receptor (EGFR) antibody was bound to LG-GFP for specific delivery to cancer cells displaying EGFR. To confirm the structural integrity of fabricated oleosome, atomic force microscopy (AFM) measurements were carried out. The oleosomes' stability is demonstrated by the homogeneous ellipsoidal structure of the phospholipid-OHNG membrane in the air which has a 276.0 nm diameter with a 5.9 nm height (Figure 1B,C). Considering that the oleosome had no supporting fluid to disperse in, the oleosome was flattened onto the substrate into an ellipsoidal structure. This typical behavior can also be seen in similar structures, including liposomes.[33] The encapsulated 8.2 ± 0.6 nm MNP inside the oleosome was also observable in the AFM image, manifesting as a 12 nm height bubble structure. From these measurements, we have calculated the expected size of the oleosomes (76.0 nm) in water by assuming the inner volume of ellipsoidal and spherical forms of the oleosome to be similar. During the synthesis process of the oleosome, we used a magnet to purify the MNP-contained oleosome and as a result of this, most of the oleosome showed the magnetic reactivity (Figure 1D). Considering olive oil's density, oleosomes are slightly lighter (0.93 g/cm^3 at 25 °C) than water (1.00 g/cm^3 at 25 °C); however, oleosomes are still able to homogeneously disperse in the solution with the mild mixing. The specific heat capacity of olive oil (1.97 kJ/(kg K)) results in another advantage for the magnetic hyperthermia application of oleosome. The magnetic oleosome showed lower specific heat capacity 3.42 ± 0.31 kJ/(kg K) relative to water (4.19 kJ/(kg K)), which is the reason why it shows a faster heating rate than water while being slower than the olive oil condition (Figure 1E).

Although recombinant oleosomes and their use as drug carriers have been previously reported,[34,35] the present study offers three important improvements over established oleosome

technology. First, oleosin proteins used to form the oleosomes are typically present as inclusion bodies in *E. coli* cell pellets.[34,35] The oleosomes containing the aforementioned oleosin fusion proteins are therefore not only prone to aggregation, but they also inevitably contain other unwanted *E. coli* hydrophobic proteins contaminants. Our approach was to guarantee homogeneity via the use of purified oleosin fusion proteins for the oleosome assembly. Hence, only the desired protein functionality is present on the oleosome surface with much less protein aggregation. Second, we created a unique coupling system that involves GFP/GFP-nanobody and protein LG/IgG binding pairs to enable simple, efficient, and universal coupling of IgG antibody to the oleosome by self-assembly. Such a strategy can be further extended by employing other binding pairs such as cellulosomal cohesion/dockerin binding domains.[22] Lastly, the oleosome system presented in the current study is endowed with magnetic susceptibility by impregnating the oil core of the oleosome with lipophilic magnetic nanoparticles, which, in turn, allows for the use of magnetic hyperthermia treatment to enhance drug release from the oleosome.

Characterization of Oleosome. The size of the prepared oleosomes was analyzed using DLS. Figure 2A shows that the oleosome diameter depends on the cycles of ultrasonication. With increasing cycles of ultrasonication, the size of the oleosome decreases up to eight cycles of ultrasonication. During the first four ultrasonication cycles, the diameter of the oleosome decreased from 500 to 200 nm. However, from 5th to 8th ultrasonication, the size of the oleosome kept almost constant near 100 nm. These last cycles instead caused a decrease in the MNP volume in the oil body, leading to an increase in oil volume and, therefore, increased carmustine loading. Due to the increase in the entire oleosome's surface area during the ultrasonication, we added additional phospholipids in the oleosome solution before the start of next cycle. During the eight cycles of ultrasonication, the surface charge of oleosomes did not change significantly (+3.3 ± 0.8 mV). Subsequently, the oleosomes were functionalized with GFP-LG and the anticancer receptor antibody, causing the size of the
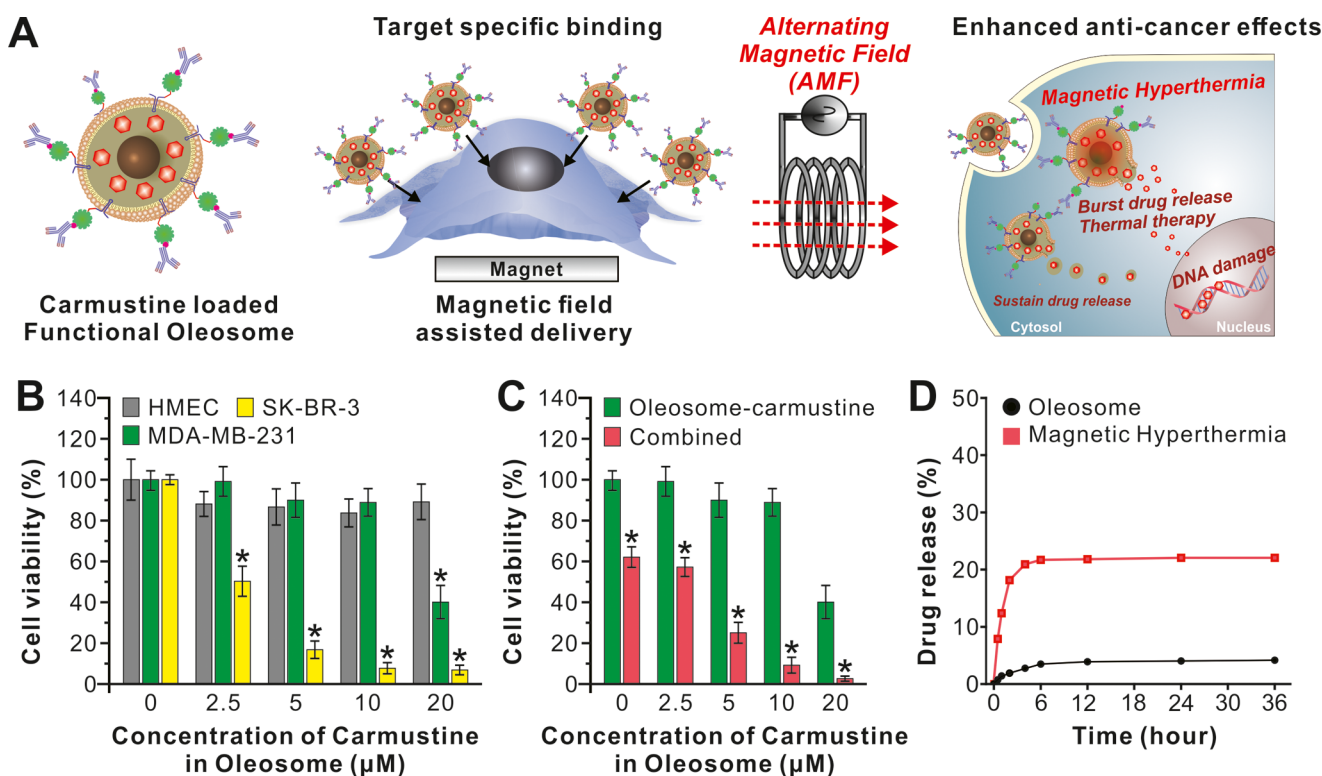
Figure 4. Synergistic anticancer effect of functional oleosome with magnetic hyperthermia. (A) Schematic illustration of functional oleosome-mediated synergistic anticancer effects by the combination of spatiotemporal heating and lipophilic drug release via magnetic hyperthermia. (B) Cell viability assay with carmustine-loaded oleosome-EGFR. Oleosome-EGFR showed target-specific anticancer effects on the EGFR-expressed cancer cells (MDA-MB-231 and SK-BR-3), whereas normal breast cell (HMEC) was not affected. (C) The cytotoxicity of MDA-MB-231 treated with combinations of carmustine and hyperthermia therapy. (D) Improved release of lipophilic fluorescence dye (drug model) from oleosome to buffer solution with magnetic hyperthermia. The dye-loaded oleosome solution was exposed to the alternating magnetic field (AMF, 45 °C, 5 min on, 2 min off, three cycles) before measuring the fluorescence intensity. Values are given as mean $\pm$ SEM ($n = 5$). *$p < 0.001$.

oleosome to increase slightly to an approximated 100 nm diameter. During the functionalization, the surface charge of oleosome was changed as a negative value with GFP-LG (-17.2 ± 1.4 mV) while slightly shifting positive after the antibody conjugation (-15.4 ± 1.6 mV). Following DLS and ζ-potential investigation, the prepared oleosomes were investigated by TEM, as demonstrated in Figure 2B. The diameter of oleosomes ultrasonicated for one and two times was shown to be 420 and 300 nm, respectively. After 5th to 8th ultrasonication cycles, the diameter of the oleosome was almost constant at about 100 nm accompanied by the drastic decrease in the MNP content. Thus, through DLS and TEM analysis, we have confirmed the successful synthesis of the functionalized oleosome.

Afterward, an mCherry (red fluorescence protein) and an anti-mCherry antibody were used to confirm the antibody-binding property of the GFP-LG protein, as well as the specificity of oleosome's delivery (Figure S3A). The IgG isotype anti-mCherry antibody and mCherry were sequentially treated on the functionalized oleosome. The mCherry-decorated oleosome showed a magnetic response by arranging along the applied magnetic field and mCherry signal was well-aligned with the GFP signal (Figure S3B).

Target-Specific Binding of Oleosome. Once the functionalized oleosomes were generated and characterized, we went on to test the delivery specificity of the lipophilic drugs and the subsequent apoptotic efficacy for two breast cancer cell lines (MDA-MB-231 and SK-BR-3), which have different surface marker expressions (Figure 3). To evaluate the targeting

property of the functionalized oleosomes with breast cancer cells, two families of oleosomes were synthesized and functionalized with appropriate antibodies—anti-epithelial growth factor receptor (EGFR) antibody and anti-human epidermal growth factor receptor 2 (HER2) antibody, respectively. Breast cancer cells were treated with the functionalized oleosomes under a magnetic field to pull down the oleosome and to increase the interactions between oleosomes and cell surface (Figure 3A,B). Two hours after treatment, fluorescent imaging clearly demonstrates a successful specific labeling of the breast cancer cells, having the expected antibody type match with the corresponding surface marker expression profile; MDA-MB-231 (EGFR$^+$/HER2$^-$) and SK-BR-3 (EGFR$^+$/HER2$^+$) (Figure 3C). The specific targeting property was also tested with normal breast cancer cells (HMECs) and neuroblastoma (SH-SY5Y), which do not express either surface markers (EGFR$^-$/HER2$^-$) (Figure S4).

Synergistic Anticancer Effects of Oleosome. To examine the cytotoxicity of the carmustine-loaded oleosomes, an MTT assay was conducted in a human mammary epithelial cell (HMEC) line as a noncancerous cell type and two breast cancer cell lines (MDA-MB-231 and SK-BR-3) (Figure 4A). The carmustine-loaded oleosomes showed significant anticancer effects on SK-BR-3 (97.2% cytotoxic effects) and MDA-MB-231 (59.9% cytotoxic effects) with 20 μM carmustine, whereas HMECs were not as significantly affected by the oleosomes, even with varying dose conditions (Figure 4B). More specifically, 26.4% of HMECs survived with the same concentration of carmustine (20 μM) under the conventional
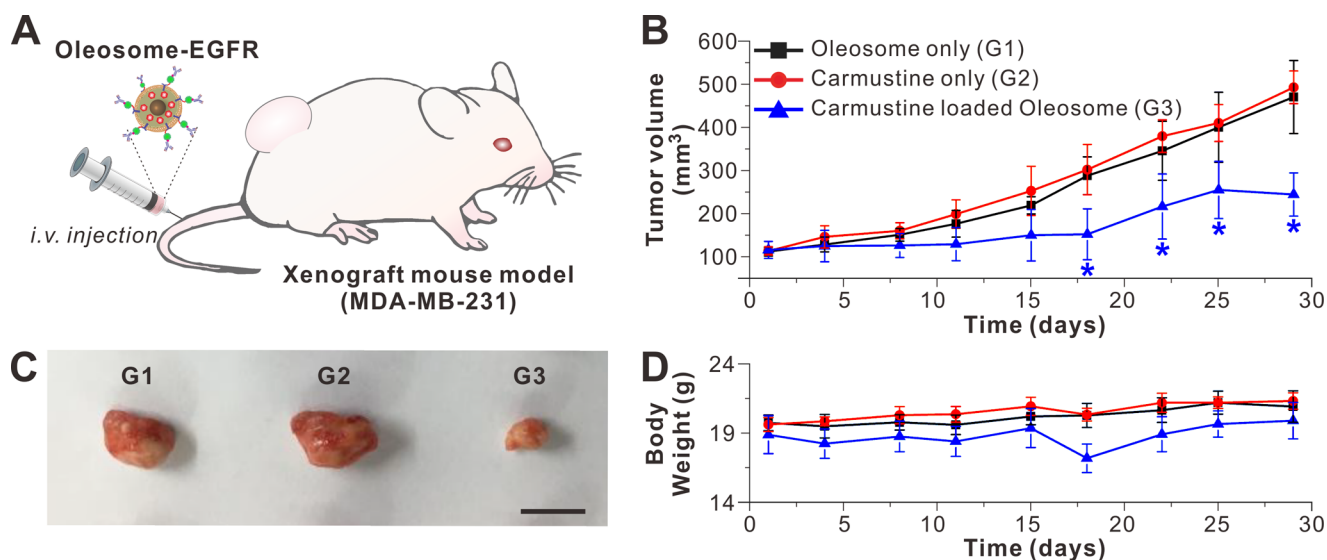
Figure 5. In vivo tumor suppression efficacy of functional oleosome. (A) Schematic illustration of functional oleosome delivery in a xenograft model. MDA-MB-231 cells were subcutaneously transplanted to generate a tumor. After tumor was formed in the mouse, EGFR-targeting oleosome (oleosome-EGFR) solution was injected intravenously. (B) Tumor growth in mice was monitored with different drug treatment conditions; PBS (control, G1), carmustine-dissolved PBS (carmustine only, G2), and carmustine-loaded oleosome (G3). Tumor volumes (mm3) were assessed with calipers and are shown as means ($n = 5$ mice per group; $*p < 0.001$ compared to G2 and G3). (C) Image of dissected tumors. The size of tumor dissected from G3 mouse showed significantly smaller size than other groups tumors (G1 and G2). Scale bar is 1 cm. (D) The whole-body weight of tested mice showed no differences between tested groups. Values are given as mean ± SEM ($n = 5$).

lipophilic drug delivery method (Figure S5A). Similarly, carmustine-loaded functional oleosomes did not show any cytotoxic effects on human umbilical vein endothelial cells even when tested with higher concentrations (50 μM), indicating that they will not be taken up by endothelial cells nonspecifically during in vivo circulation (Figure S5B). Consequently, our oleosome platform has shown selective and effective anticancer treatment results; however, in the case of MDA-MB-231, the efficacy needs improvement. We hypothesize that MDA-MB-231 shows enhanced drug resistance due to a higher expression of drug efflux transporter genes (ABCG2) compared to other breast cancer cell lines such as SK-BR-3; hence, we consider the treatment of higher concentrations or conducting additional treatment methods.[36]

Finally, owing to the magnetic properties of our oleosomes, the oleosome can provide many desirable advantageous functionalities. For instance, previous studies from our group[24,25,37] and others[38−40] have demonstrated the ability of MNPs to induce localized and effective magnetically induced hyperthermia, which partially acts by targeting DNA repair mechanisms as well as directly inducing apoptosis. To this end, we hypothesized that the combination of magnetic hyperthermia together with the carmustine could be used to generate the desired synergistic DNA damage and apoptosis in cancer cells. Moreover, by using a single MNP core, we not only could induce magnetic hyperthermia but also facilitate drug release from the oil phase to the water phase, which is a significant limitation of the traditional oil-based drug delivery (Figure 4A). The oleosome showed approximately 40% killing efficiency with magnetic hyperthermia when compared to similar concentrations of the carmustine oleosome conditions (Figure 4C). Moreover, 5 and 10 μM concentrations of carmustine-loaded oleosomes show an enhancement of up to approximately 80% killing efficiency. Through a phase-transfer drug-monitoring system based on a lipophilic fluorescent dye (SP-DiOC$_{18}$(3)), we confirmed that this synergistic effect was due

to the ability of magnetic hyperthermia to further improve the drug transfer from the oil to water phase (Figure 4D).[41]

Evaluation of in Vivo Anticancer Activity. After confirming our strategy in in vitro cultures of cancer cell lines, we next sought to confirm the biocompatibility as well as the tumor suppression efficacy of the oleosome toward a xenograft mouse model with malignant breast cancer cells (MDA-MB-231) (Figure 5). To achieve this goal, the toxicity of carmustine on the mouse, where carmustine was introduced via intravenous injection with different doses, was determined before therapeutic efficacy investigation. Carmustine is a known cell cycle phase nonspecific alkylating antineoplastic agent. Not only does carmustine have a high lipid solubility, but it also has been shown to readily cross the blood−brain barrier, leading it to become one of the most clinically used drugs for brain tumor treatment.[42] However, it is not popularly used for other malignant tumors due to its lack of target specificity and easy cell membrane fusion in normal tissues during regular body circulation.[43] By varying the volume ratio of oleosome, we found that 1:50 (oleosome/PBS) or less ratio of oleosome solution had a negligible effect on survivability under the daily intravenous injection condition, whereas over 1:10 ratio of oleosome solution was found to be toxic after 1 h injection by the obstruction of blood flow.

After the confirmation of the optimum ratio of oleosomes for the mouse model, carmustine-loaded oleosomes were administered to mouse via intravenous injection to confirm the tumor suppression effects of carmustine (Figure 5A). Specifically, 4 weeks after the injection, we confirmed that carmustine-loaded oleosomes showed a significant tumor inhibition (69.7% suppression in tumor volume vs. control group), whereas single treatment of carmustine showed a 5.9% increase in tumor volume instead (Figure 5B,C). Additionally, no damage to other organs (e.g., liver, kidney, spleen, data not shown) and consistent body weight increase were observed (Figure 5D), proving that the oleosome effectively delivered the carmustine

into the tumor specifically for tumor ablation. This provides a successful proof-of-concept test that functional oleosomes can be an attractive candidate for target specific lipophilic drug delivery with minimal side effects to normal/healthy cells.

CONCLUSIONS

In this study, an oleosome-containing magnetic nanoparticles and drugs was developed as an effective lipid-based lipophilic drug delivery agent. To effectively target cancer cells, the oleosome boundary protein, oleosin, was modified to link with an anti-GFP nanobody via a recombinant DNA technique, and a recombinant protein (GFP-LG) was successfully used to couple the oleosome with an antibody for cancer cell surface receptor targeting. The AFM analysis confirmed the correct assembly of the antibody-functionalized oleosomes, and the lipid core of the oleosome was successfully loaded with carmustine and magnetic nanoparticles. The functionalized magnetic oleosomes showed a high selectivity toward cancer cells with a high anticancer activity in cancer cell cultures due in part to the ability of magnetic hyperthermia to improve drug release. Furthermore, the in vivo animal study also supports the efficacy of the magnetic oleosome delivery system. Taken together, the proposed oleosome system provides a versatile and effective drug delivery system with a great potential for advancing breast cancer treatment.

ASSOCIATED CONTENT

Supporting Information

The Supporting Information is available free of charge on the ACS Publications website at DOI: 10.1021/acsami.7b19255.

> STEM images and X-ray diffraction patterns of $ZnFe_2O_4$ nanoparticles, EDX results of $ZnFe_2O_4$ and Fe_3O_4 nanoparticles, and magnetic response and target specific delivery of carmustine with oleosome (PDF)

AUTHOR INFORMATION

Corresponding Authors

*E-mail: wsu@hawaii.edu. Tel: (+1) 808-956-3531. Fax: (+1) 808-956-3542 (W.W.S.).
*E-mail: jwchoi@sogang.ac.kr. Tel: (+82) 2-705-8480. Fax: (+82) 2-3273-0331 (J.-W.C.).

ORCID

Jeong-Woo Choi: 0000-0003-0100-0582

Author Contributions

#H.-Y.C. and T.L. contributed equally to this work. The manuscript was written through contributions of all authors. H.-Y.C. and J.-W.C. designed the project. H.-Y.C., T.L., J.Y., H.R., and K.-B.L. synthesized and characterized the oleosome. Z.H. and W.W.S. engineered proteins. H.-Y.C. and T.L. conducted in vitro and in vivo experiments and analysis.

Notes

The authors declare no competing financial interest.

ACKNOWLEDGMENTS

REFERENCES

(1) Porter, C. J. H.; Trevaskis, N. L.; Charman, W. N. Lipids and Lipid-Based Formulations: Optimizing the Oral Delivery of Lipophilic Drugs. *Nat. Rev. Drug Discovery* **2007**, *6*, 231−248.

(2) Savjani, K. T.; Gajjar, A. K.; Savjani, J. K. Drug Solubility: Importance and Enhancement Techniques. *ISRN Pharm.* **2012**, *2012*, No. 195727.

(3) Dehghani, F.; Farhadian, N.; Golmohammadzadeh, S.; Biriaee, A.; Ebrahimi, M.; Karimi, M. Preparation, Characterization and in-Vivo Evaluation of Microemulsions Containing Tamoxifen Citrate Anti-Cancer Drug. *Eur. J. Pharm. Sci.* **2017**, *96*, 479−489.

(4) Airan, R. D.; Meyer, R. A.; Ellens, N. P.; Rhodes, K. R.; Farahani, K.; Pomper, M. G.; Kadam, S. D.; Green, J. J. Noninvasive Targeted Transcranial Neuromodulation Via Focused Ultrasound Gated Drug Release from Nanoemulsions. *Nano Lett.* **2017**, *17*, 652−659.

(5) Singh, Y.; Meher, J. G.; Raval, K.; Khan, F. A.; Chaurasia, M.; Jain, N. K.; Chourasia, M. K. Nanoemulsion: Concepts, Development and Applications in Drug Delivery. *J. Controlled Release* **2017**, *252*, 28−49.

(6) Crum, M. F.; Trevaskis, N. L.; Williams, H. D.; Pouton, C. W.; Porter, C. J. A New in Vitro Lipid Digestion-in Vivo Absorption Model to Evaluate the Mechanisms of Drug Absorption from Lipid-Based Formulations. *Pharm. Res.* **2016**, *33*, 970−982.

(7) Tran, T.; Xi, X.; Rades, T.; Müllertz, A. Formulation and Characterization of Self-Nanoemulsifying Drug Delivery Systems Containing Monoacyl Phosphatidylcholine. *Int. J. Pharm.* **2016**, *502*, 151−160.

(8) Meng, J.; Guo, F.; Xu, H.; Liang, W.; Wang, C.; Yang, X. D. Combination Therapy Using Co-Encapsulated Resveratrol and Paclitaxel in Liposomes for Drug Resistance Reversal in Breast Cancer Cells in Vivo. *Sci. Rep.* **2016**, *6*, No. 22390.

(9) Zhang, X.; Li, N.; Liu, Y.; Ji, B.; Wang, Q.; Wang, M.; Dai, K.; Gao, D. On-Demand Drug Release of Icg-Liposomal Wedelolactone Combined Photothermal Therapy for Tumor. *Nanomedicine* **2016**, *12*, 2019−2029.

(10) Lu, M.; Xiong, D.; Sun, W.; Yu, T.; Hu, Z.; Ding, J.; Cai, Y.; Yang, S.; Pan, B. Sustained Release Ivermectin-Loaded Solid Lipid Dispersion for Subcutaneous Delivery: In Vitro and in Vivo Evaluation. *Drug Delivery* **2017**, *24*, 622−631.

(11) Zhao, Y.; Chang, Y. X.; Hu, X.; Liu, C. Y.; Quan, L. H.; Liao, Y. H. Solid Lipid Nanoparticles for Sustained Pulmonary Delivery of Yuxingcao Essential Oil: Preparation, Characterization and in Vivo Evaluation. *Int. J. Pharm.* **2017**, *516*, 364−371.

(12) Ciocci, M.; Iorio, E.; Carotenuto, F.; Khashoggi, H. A.; Nanni, F.; Melino, S. H_2S-Releasing Nanoemulsions: A New Formulation to Inhibit Tumor Cells Proliferation and Improve Tissue Repair. *Oncotarget* **2016**, *7*, 84338−84358.

(13) Plaza-Oliver, M.; Baranda, J. F.; Rodriguez Robledo, V.; Castro-Vazquez, L.; Gonzalez-Fuentes, J.; Marcos, P.; Lozano, M. V.; Santander-Ortega, M. J.; Arroyo-Jimenez, M. M. Design of the Interface of Edible Nanoemulsions to Modulate the Bioaccessibility of Neuroprotective Antioxidants. *Int. J. Pharm.* **2015**, *490*, 209−218.

(14) Sandhu, P. S.; Kumar, R.; Beg, S.; Jain, S.; Kushwah, V.; Katare, O. P.; Singh, B. Natural Lipids Enriched Self-Nano-Emulsifying Systems for Effective Co-Delivery of Tamoxifen and Naringenin: Systematic Approach for Improved Breast Cancer Therapeutics. *Nanomedicine* **2017**, *13*, 1703−1713.

(15) Akbarzadeh, A.; Rezaei-Sadabady, R.; Davaran, S.; Joo, S. W.; Zarghami, N.; Hanifehpour, Y.; Samiei, M.; Kouhi, M.; Nejati-Koshki, K. Liposome: Classification, Preparation, and Applications. *Nanoscale Res. Lett.* **2013**, *8*, No. 102.

(16) Joshi, S.; Hussain, M. T.; Roces, C. B.; Anderluzzi, G.; Kastner, E.; Salmaso, S.; Kirby, D. J.; Perrie, Y. Microfluidics Based Manufacture of Liposomes Simultaneously Entrapping Hydrophilic and Lipophilic Drugs. *Int. J. Pharm.* **2016**, *514*, 160−168.

(17) Waschatko, G.; Junghans, A.; Vilgis, T. A. Soy Milk Oleosome Behaviour at the Air-Water Interface. *Faraday Discuss.* **2012**, *158*, 157−169.

(18) Ichihara, K. Lipid-Metabolism in Safflower.5. Formation of Oleosomes in Maturing Safflower Seeds. *Agric. Biol. Chem.* **1982**, *46*, 1767−1773.

(19) Maurer, S.; Waschatko, G.; Schach, D.; Zielbauer, B. I.; Dahl, J.; Weidner, T.; Bonn, M.; Vilgis, T. A. The Role of Intact Oleosin for Stabilization and Function of Oleosomes. *J. Phys. Chem. B* **2013**, *117*, 13872−13883.

(20) Kapchie, V. N.; Wei, D.; Hauck, C.; Murphy, P. A. Enzyme-Assisted Aqueous Extraction of Oleosomes from Soybeans (Glycine Max). *J. Agric. Food Chem.* **2008**, *56*, 1766−1771.

(21) Han, Z.; Zhang, B.; Wang, Y. E.; Zuo, Y. Y.; Su, W. W. Self-Assembled Amyloid-Like Oligomeric-Cohesin Scaffoldin for Augmented Protein Display on the Saccharomyces Cerevisiae Cell Surface. *Appl. Environ. Microbiol.* **2012**, *78*, 3249−3255.

(22) Han, Z.; Madzak, C.; Su, W. W. Tunable Nano-Oleosomes Derived from Engineered Yarrowia Lipolytica. *Biotechnol. Bioeng.* **2013**, *110*, 702−710.

(23) Kihlberg, B. M.; Sjobring, U.; Kastern, W.; Bjorck, L. Protein Lg: A Hybrid Molecule with Unique Immunoglobulin Binding Properties. *J. Biol. Chem.* **1992**, *267*, 25583−25588.

(24) Yin, P. T.; Shah, B. P.; Lee, K. B. Combined Magnetic Nanoparticle-Based Microrna and Hyperthermia Therapy to Enhance Apoptosis in Brain Cancer Cells. *Small* **2014**, *10*, 4106−4112.

(25) Shah, B. P.; Pasquale, N.; De, G.; Tan, T.; Ma, J.; Lee, K. B. Core-Shell Nanoparticle-Based Peptide Therapeutics and Combined Hyperthermia for Enhanced Cancer Cell Apoptosis. *ACS Nano* **2014**, *8*, 9379−9387.

(26) Shah, B.; Yin, P. T.; Ghoshal, S.; Lee, K. B. Multimodal Magnetic Core-Shell Nanoparticles for Effective Stem-Cell Differentiation and Imaging. *Angew. Chem., Int. Ed.* **2013**, *52*, 6190−6195.

(27) Sun, S.; Zeng, H.; Robinson, D. B.; Raoux, S.; Rice, P. M.; Wang, S. X.; Li, G. Monodisperse Mfe2o4 (M = Fe, Co, Mn) Nanoparticles. *J. Am. Chem. Soc.* **2004**, *126*, 273−279.

(28) Jang, J. T.; Nah, H.; Lee, J. H.; Moon, S. H.; Kim, M. G.; Cheon, J. Critical Enhancements of Mri Contrast and Hyperthermic Effects by Dopant-Controlled Magnetic Nanoparticles. *Angew. Chem., Int. Ed.* **2009**, *48*, 1234−1238.

(29) Dong, A.; Ye, X.; Chen, J.; Kang, Y.; Gordon, T.; Kikkawa, J. M.; Murray, C. B. A Generalized Ligand-Exchange Strategy Enabling Sequential Surface Functionalization of Colloidal Nanocrystals. *J. Am. Chem. Soc.* **2011**, *133*, 998−1006.

(30) Duchowicz, P. R.; Talevi, A.; Bruno-Blanch, L. E.; Castro, E. A. New Qspr Study for the Prediction of Aqueous Solubility of Drug-Like Compounds. *Bioorg. Med. Chem.* **2008**, *16*, 7944−7955.

(31) Szczerba, W.; Zukrowski, J.; Przybylski, M.; Sikora, M.; Safonova, O.; Shmeliov, A.; Nicolosi, V.; Schneider, M.; Granath, T.; Oppmann, M.; Strasser, M.; Mandel, K. Pushing up the Magnetisation Values for Iron Oxide Nanoparticles Via Zinc Doping: X-Ray Studies on the Particle's Sub-Nano Structure of Different Synthesis Routes. *Phys. Chem. Chem. Phys.* **2016**, *18*, 25221−25229.

(32) Tatarchuk, T.; Bououdina, M.; Macyk, W.; Shyichuk, O.; Paliychuk, N.; Yaremiy, I.; Al-Najar, B.; Pacia, M. Structural, Optical, and Magnetic Properties of Zn-Doped Cofe 2 O 4 Nanoparticles. *Nanoscale Res. Lett.* **2017**, *12*, No. 141.

(33) Zhang, Y.; Cheng, C. M.; Cusick, B.; LeDuc, P. R. Chemically Encapsulated Structural Elements for Probing the Mechanical Responses of Biologically Inspired Systems. *Langmuir* **2007**, *23*, 8129−8134.

(34) Chiang, C. J.; Chen, H. C.; Chao, Y. P.; Tzen, J. T. Efficient System of Artificial Oil Bodies for Functional Expression and Purification of Recombinant Nattokinase in *Escherichia Coli. J. Agric. Food Chem.* **2005**, *53*, 4799−4804.

(35) Chiang, C. J.; Chen, C. J.; Lin, L. J.; Chang, C. H.; Chao, Y. P. Selective Delivery of Cargo Entities to Tumor Cells by Nanoscale Artificial Oil Bodies. *J. Agric. Food Chem.* **2010**, *58*, 11695−11702.

(36) Palasuberniam, P.; Yang, X.; Kraus, D.; Jones, P.; Myers, K. A.; Chen, B. Abcg2 Transporter Inhibitor Restores the Sensitivity of Triple Negative Breast Cancer Cells to Aminolevulinic Acid-Mediated Photodynamic Therapy. *Sci. Rep.* **2015**, *5*, No. 13298.

(37) Yin, P. T.; Shah, S.; Pasquale, N. J.; Garbuzenko, O. B.; Minko, T.; Lee, K. B. Stem Cell-Based Gene Therapy Activated Using Magnetic Hyperthermia to Enhance the Treatment of Cancer. *Biomaterials* **2016**, *81*, 46−57.

(38) Chatterjee, D. K.; Diagaradjane, P.; Krishnan, S. Nanoparticle-Mediated Hyperthermia in Cancer Therapy. *Ther. Delivery* **2011**, *2*, 1001−1014.

(39) Bañobre-López, M.; Teijeiro, A.; Rivas, J. Magnetic Nano-particle-Based Hyperthermia for Cancer Treatment. *Rep. Pract. Oncol. Radiother.* **2013**, *18*, 397−400.

(40) Hervault, A.; Thanh, N. T. Magnetic Nanoparticle-Based Therapeutic Agents for Thermo-Chemotherapy Treatment of Cancer. *Nanoscale* **2014**, *6*, 11553−11573.

(41) Van, J. B. B.; De Boer, A. G.; Danhof, M.; Breimer, D. D. Drug Transport across the Blood-Brain Barrier. Iii. Mechanisms and Methods to Improve Drug Delivery to the Central Nervous System. *Pharm. World Sci.* **1993**, *15*, 2−9.

(42) Zhan, W.; Arifin, D. Y.; Lee, T. K.; Wang, C. H. Mathematical Modelling of Convection Enhanced Delivery of Carmustine and Paclitaxel for Brain Tumour Therapy. *Pharm. Res.* **2017**, *34*, 860−873.

(43) Kari, P.; McConnell, W. R.; Finkel, J. M.; Hill, D. L. Distribution of Bratton-Marshall-Positive Material in Mice Following Intravenous Injections of Nitrosoureas. *Cancer Chemother. Pharmacol.* **1980**, *4*, 243−248.